
HIERARCHICAL MULTI-STAGE TRANSFORMER ARCHITECTURE FOR CONTEXT-AWARE TEMPORAL ACTION LOCALIZATION

Hayat Ullah¹, Arslan Munir¹, and Oliver Nina²

¹Department of Electrical Engineering and Computer Science, Florida Atlantic University

²Air Force Research Laboratory

¹{hullah2024, arslanm}@fau.edu

²oliver.nina.1@afrl.af.mil

ABSTRACT

Inspired by the recent success of transformers and multi-stage architectures in video recognition and object detection domains. We thoroughly explore the rich spatio-temporal properties of transformers within a multi-stage architecture paradigm for the temporal action localization (TAL) task. This exploration led to the development of a hierarchical multi-stage transformer architecture called PCL-Former, where each subtask is handled by a dedicated transformer module with a specialized loss function. Specifically, the Proposal-Former identifies candidate segments in an untrimmed video that may contain actions, the Classification-Former classifies the action categories within those segments, and the Localization-Former precisely predicts the temporal boundaries (i.e., start and end) of the action instances. To evaluate the performance of our method, we have conducted extensive experiments on three challenging benchmark datasets: THUMOS-14, ActivityNet-1.3, and HACS Segments. We also conducted detailed ablation experiments to assess the impact of each individual module of our PCL-Former. The obtained quantitative results validate the effectiveness of the proposed PCL-Former, outperforming state-of-the-art TAL approaches by 2.8%, 1.2%, and 4.8% on THUMOS14, ActivityNet-1.3, and HACS datasets, respectively.

1 INTRODUCTION

Temporal action localization (TAL) plays a key role in understanding the context of long videos containing both action-specific and background scenes. TAL in untrimmed videos involves identifying and localizing actions within a video timeline without prior segmentation or labeling. It's a critical task in video understanding to precisely determine actions' occurrence and their duration within long untrimmed video sequences. However, temporal localization of action-specific scenes in untrimmed videos is a challenging problem due to various complexities. One of the primary challenges lies in the inherent variability of actions within untrimmed videos. Actions can occur in different temporal extents, speeds, and occlusions, making their accurate detection and localization a formidable task. This variability necessitates models capable of handling these nuances while discerning actions from complex backgrounds, diverse contexts, and occluded instances, thereby demanding robustness and adaptability from TAL algorithms.

To address these challenges, various TAL approaches have been developed, broadly categorized into three types: (1) *Anchor-based*, (2) *Actionness-guided*, and (3) *Anchor-free* approaches. Anchor-based methods Chao et al. (2018); Gao et al. (2017); Xu et al. (2017) generate action proposals using predefined anchors across temporal scales, followed by classification and boundary regression. Contrarily, Actionness-guided methods Lin et al. (2018; 2019) predict action-start, action-end probabilities, and duration to form proposals without predefined anchors. Anchor-free methods Lin et al. (2021); Ou et al. (2022) generate proposals at each temporal position by

associating the start and end of action, reducing proposal redundancy and computational overhead compared to action-ness-guided approaches.

We observe several notable limitations in existing TAL approaches. First, anchor-based methods Chao et al. (2018); Gao et al. (2017); Xu et al. (2017) rely on predefined anchors, limiting their adaptability to varying action lengths and making them sensitive to hyper-parameters. Second, actionness-guided methods Lin et al. (2018; 2019) remove this dependency but introduce significant computational overhead due to the need for an additional classification model. Third, Anchor-free approaches Lin et al. (2021); Ou et al. (2022) reduce redundancy and computational cost yet may struggle with long-range temporal dependencies and handling actions of varying durations. Overall, these methods face challenges in balancing accuracy, efficiency, and adaptability across different action categories and temporal scales.

Inspired by the recent success of multi-stage transformer architectures in the object detection domain Zhang et al. (2023), we thoroughly explore transformer for temporal action localization task and propose three-tier transformer architecture named PCL-Former. Unlike existing TAL methods, which utilize pre-trained video encoders, these models fail to fully leverage the inherent semantic information due to limited feature representation. Specifically, video encoders pre-trained for video-level classification are not optimized for the TAL task, resulting in snippet-level features that lack sufficient contextual information for precise action localization. Our PCL-Former is designed to address three core subtasks of TAL using distinct transformer modules. The Proposal-Former identifies candidate segments that may potentially contain actions and eliminates background segments. The Classification-Former classifies the action category in a given segment. It is worth mentioning here that the classification network focuses on categorizing action instances rather than accurately localizing their temporal boundaries. In some cases, high classification scores may be assigned to segments with minimal overlap with the ground truth, which can be problematic. Post-processing techniques like Non-Maximum Suppression (NMS) may discard segments with small scores but significant overlap with the ground truth. To address this, we introduce the Localization-Former, equipped with a specialized loss function that prioritizes segments with higher temporal overlap. This encourages more reliable confidence scores for downstream post-processing, improving action localization accuracy.

More precisely, the main **contributions** of this paper are the following: (1) To overcome the fundamental limitations of mainstream TAL methods, such as limited adaptability to varying action lengths, high computational overhead of independently trainable modules, and challenges with long-range temporal dependencies, we leverage the rich spatio-temporal modeling capabilities of transformers and multi-stage architectures for the temporal action localization task. (2) We propose PCL-Former, an effective three-tier transformer architecture designed to handle the key subtasks of TAL with specialized transformer modules, each guided by a task-specific loss function. Specifically, the Proposal-Former generates candidate segments likely to contain actions, the Classification-Former categorizes actions in a given segment, and the Localization-Former predicts the temporal boundaries of actions within the segment. During testing, the Proposal-Former effectively filters out background segments, enhancing overall performance. (3) The proposed method is extensively evaluated on three benchmark datasets commonly used for the temporal action localization task. The obtained quantitative results validate the effectiveness of the proposed PCL-Former, outperforming state-of-the-art TAL approaches by 2.8%, 1.2%, and 4.8% on THUMOS14, ActivityNet-1.3, and HACS datasets, respectively.

2 RELATED WORK

Action Recognition: In the realm of video comprehension, action recognition stands as a fundamental task, significantly advanced by deep learning methods. Leveraging 2D and 3D CNNs Tran et al. (2015); Carreira & Zisserman (2017); Wang et al. (2016); Tran et al. (2018) has notably boosted performance on standard action recognition benchmarks. More recently, Vision Transformer-based approaches Bertasius et al. (2021); Liu et al. (2022b); Fan et al. (2021) have shown considerable superiority over previous CNN-based methods. These Vision Transformer models, benefiting from extensive pre-training on action recognition datasets, are commonly employed as short-term feature extractors in temporal action localization tasks. However, a

drawback of these contemporary video transformer models is their slower training pace and hefty GPU memory requirements due to the quadratic memory complexity of self-attention mechanisms Vaswani et al. (2017). Consequently, their effective application to long-term modeling tasks, such as temporal action localization, poses notable challenges.

Temporal Action Localization: The temporal action localization approaches Zhao et al. (2022); Faure et al. (2023); Lin et al. (2017); Long et al. (2019); Xu et al. (2017); Chao et al. (2018) fall into two distinct classes that include *Single-Stage TAL* and *Two-Stage TAL* approaches. The *Single-Stage TAL* methods localize actions in a video without any action proposal, generating anchors using a sliding window. The SSAD Lin et al. (2017) and GTAN Long et al. (2019) are Single-Stage methods. The SSAD Lin et al. (2017) employed a single-shot structure using 1D convolution to generate anchors for temporal action localization, while GTAN Long et al. (2019) utilized a 3D ConvNet to extract fine-grained segment-level features. GTAN further employs temporal Gaussian kernels to generate proposals with varying temporal resolutions. On the other hand, Two-Stage TAL approaches Xu et al. (2017); Chao et al. (2018) first generate candidate segments from input video as action proposals and then classify them into actions and refine their temporal boundaries. The R-C3D Xu et al. (2017) method integrates candidate segment generation and classification within an end-to-end network, allowing input videos of varying lengths. TALNet Chao et al. (2018) specifically focused on expanding the receptive field for feature extraction and incorporates temporal context extraction alongside late fusion in a two-stream architecture.

Transformers in Videos: The transformer architecture, originally introduced for the Natural Language Processing (NLP) task in Vaswani et al. (2017) reliant on self-attention mechanisms to capture sequence relationships, has recently gained substantial interest in computer vision. Specifically, the self-attention mechanism within transformers has emerged as a pivotal tool for extracting temporal information from videos. In object detection, DETR Carion et al. (2020) innovatively employed object queries instead of traditional anchors as candidates. Yet, for action detection, a pure transformer architecture might prove insufficient in handling intricate temporal dependencies. MS-TCT Dai et al. (2022), recognizing this limitation, incorporates convolutions to enable multiple temporal scales of tokens, ensuring temporal consistency and integrating local information between tokens. In the domain of Temporal Action Localization, ATAG Chang et al. (2022) introduces an augmented transformer with an adaptive graph network, capturing both long-term and local temporal context for enhanced understanding. Similarly, TAPG Wang et al. (2021b) devises a unified framework comprising boundary and proposal transformers, each focusing on long-term dependencies and proposal relationship enrichment, ensuring accurate boundary prediction and reliable confidence assessment. Inspiring from ViT Dosovitskiy et al. (2020), ViViT Arnab et al. (2021) introduced a factorized encoder model a fusion of spatial and temporal transformer encoders to model diverse temporal interactions, enhancing spatial-temporal understanding.

3 OUR METHOD

In this section, we provide the problem formulation and a detailed explanation of our proposed PCLFormer architecture. The detailed visual overview of our proposed method is depicted in Figure 1.

3.1 PROBLEM FORMULATION

The temporal action localization task involves two sub-tasks: action category classification and action interval (start and end timestamps of action instance) prediction in a given untrimmed video. To better formulate this problem, consider a given untrimmed video $\mathbf{X} \in \mathbb{R}^{3 \times H \times W \times T}$, where H and W are the height and width, and T is the number of frame or temporal length. The temporal actions can be denoted as $\Psi_g = \{\varphi_i = (t_s, t_e, c)\}_{i=1}^N$, where t_s, t_e, c are the start, end time and category of action instance φ_i , and N is the number of actions in a given untrimmed video. Further, the action instance φ_i starts at time $\varphi_i^{t_s}$ that is $(0 \leq \varphi_i^{t_s} < N)$ and ends at time $\varphi_i^{t_e}$ that is $(0 < \varphi_i^{t_e} \leq N)$. Thus, our objective is to predict the category c of action instance φ_i and its occurrence interval $(t_s$ and $t_e)$ in a given untrimmed video.

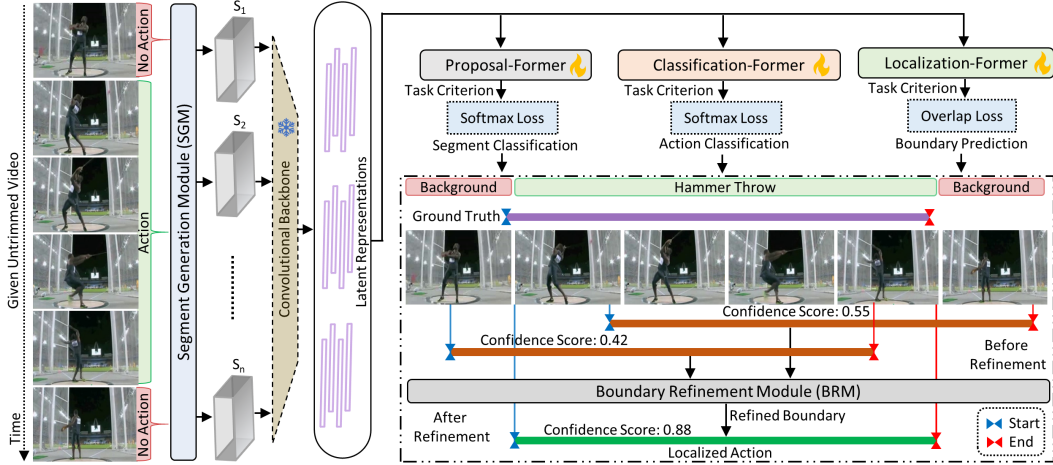


Figure 1: Visual overview of our proposed PCL-Former. The input untrimmed video is divided into fixed-size segments by the SGM module. These segments are passed to a convolutional backbone for video-level feature extraction. The latent representations are then fed into sub-task transformers. The outputs (action class and boundaries) are refined by the BRM module to produce the final predictions.

3.2 PCL-FORMER

In pursuit of this objective, we propose a three-tier transformer architecture called PCL-Former for solving three distinct tasks inspired by Shou et al. (2016). *Proposal-Former* for generating candidate segments, *Classification-Former* for action instance classification, and *Localization-Former* for action boundary prediction. Besides, our PCL-Former includes a pre-processing module called *Segment Generation Module* (SGM) that segments the input untrimmed video in multiple segments. The convolutional backbone extracts video-level features from input segments. A post-processing module called *Boundary Refinement Module* (BRM) for refining the predicted boundaries for precise localization of action instances.

It is worth mentioning here that each sub-network of PCL-Former utilizes the ViViT-like architecture Arnab et al. (2021) due to its overwhelming performance on video classification tasks. However, instead of standard multi-head self-attention, we use factorized self-attention as it reduces the quadratic complexity of computing attention scores to linear complexity, making it more scalable for long sequences. This is achieved by decomposing the attention computation into smaller, more manageable steps, which decreases computational and memory overhead while maintaining the overall model’s performance.

Segment Generation Module: Given an untrimmed video $\mathcal{V} = \sum_{i=1}^N (f_i)$, we divide it into fixed size (64 frames per segment) multiple segments $\mathcal{S} = \{s_1, s_2, \dots, s_n\}$, by traversing temporal sliding window over the length of \mathcal{V} , having 50% overlap between two consecutive segments, where the frame resolution; height \mathcal{H} and width \mathcal{W} are set to 224 and 224, respectively. Thus for each untrimmed video \mathcal{V} , we get a list of candidate segments \mathcal{S} , where each segment has a length of 64 frames having a resolution of (224×224) with 50% frames from the previous segment.

$$\mathcal{S}\{s_1, s_2, \dots, s_n\} = \sum_{i=1}^N SGM(\mathcal{V})_r^t \quad (1)$$

Where t is the temporal length of each segment (i.e., 64) and r is the resolution (i.e., 224×224) of frames in each segment.

Proposal-Former: The main objective of *Proposal-Former* Θ_{PF} in this study is to filter the input segment for background and action instances. To prepare the training data for Θ_{PF} , we follow the data preparation protocol given in Shou et al. (2016). Let, $D_{prop}^{train} = \{(s_i, c_i)\}$, where $c_i \in \{0,1\}$ is the action category of i^{th} instance.

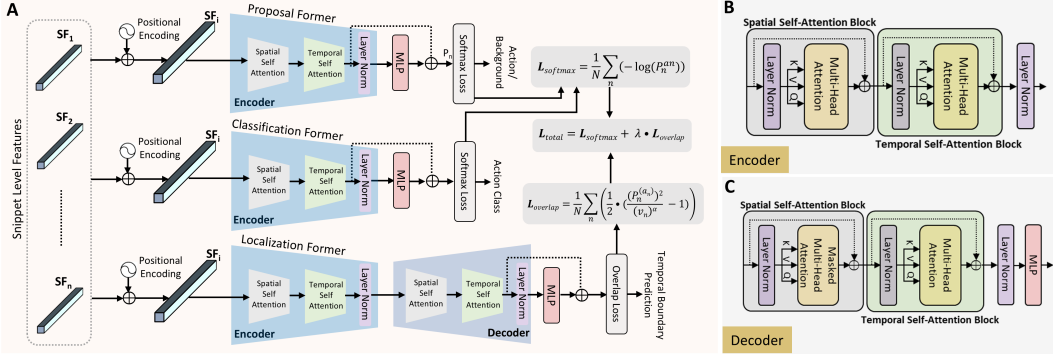


Figure 2: The detailed architectural overview of our **PCL-Former**: (A) Depicts the complete workflow of training protocol of our entire architecture, processing the input features through **Proposal Former**, **Classification Former**, and **Localization Former** equipped with task-specific loss functions. Moreover, (B) depicts the block diagram of **Encoder** module used in each sub-network and (C) depicts the block diagram of **Decoder** module used in Localization Former.

For a given set of segments \mathcal{S} of an untrimmed video \mathcal{V} along with its temporal annotation \mathcal{A} , labels are assigned to each segment by evaluating its overlap with the ground truth using Intersection Over Union (IoU). Segments having IoU greater than 0.7 are labeled as positive and lower than 0.3 are labeled as negative. Given the input set of segments \mathcal{S} from D_{prop}^{train} , we extract features using convolutional backbone (TSN Wang et al. (2016) and I3D Carreira & Zisserman (2017)). the Θ_{PF} performs linear positional encoding on the extracted features and passes it to the sequential multi-head self-attention blocks, where each block contains a multi-head attention layer, normalization layer, and MLP block. The output embedding of the MLP block is then passed to *softmax* layer for binary classification (i.e., background (b) or action (a)).

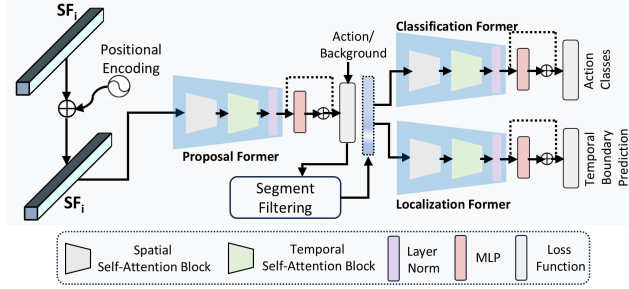


Figure 3: The detailed inference workflow of our **PCL-Former** architecture: the **Proposal Former** identifies candidate segment features (SF_i), segment filtering discards background segments, and only positive (action-containing) segments are passed to the **Classification Former** and **Localization Former** for action classification and temporal boundary prediction.

Classification-Former: The *Classification-Former* Θ_{CF} has the same architecture as the *Proposal-Former* except the last layer, as shown in Figure 2. Unlike the previous task, where the goal is to differentiate between background and action scenes. Here the objective of *Classification-Former* is to not only differentiate between background and action scenes but also predict the category label of action in the presence of action (a_c , $c \in [1, 2, \dots, \mathcal{C}]$). Where \mathcal{C} is the number of action classes. Training data for Θ_{CF} is prepared using the same approach as for Θ_{PF} . Except with one change, when labeling positive segments, each segment is labeled with an action category.

Localization-Former: The *Localization-Former* Θ_{LF} operates on the input segments and prioritizes segments with higher overlap with the ground truth instances. Elevating the prediction score \mathcal{P} for segments that closely align with the ground truth and reducing scores for those with lesser overlap using overlap loss given in Eq.3, which ensures a refined selection process in the subsequent post-processing steps. The Θ_{LF} is trained on temporally annotated data D_{Loc}^{train} , prepared by associating each segment $s \in \mathcal{S}$ with its overlap v . If a given segment s has positive action $a \in \mathcal{A}$, v is assigned with the overlap value between the segment s and its corresponding ground truth \mathcal{GT} . If a segment s is a background segment, we set v equal to 0. The encoder part of Θ_{LF} is the same as Proposal- and Classification-Former, except MLP block, which is excluded, as depicted in Figure 2(A). On the other hand, in the decoder architecture, we replaced the spatial

multi-head self-attention with multi-head masked self-attention, as shown in Figure 2(C). The temporal multi-head self-attention is used as it is used in the encoder. Upon receiving the encoded representations from the encoder, the decoder employs masked multi-head self-attention to manage both current and preceding outputs.

Boundary Refinement Module: The boundary refinement module is used as a post-processing module for filtering the predicted actions and their boundaries (confidence score). The BRM module first eliminates all segments having less overlap with ground truth. Then it proceeds to enhance the remaining segments by cross-referencing them with the occurrence of actions within the corresponding time intervals. Finally, the redundant detections (temporal boundaries) are removed using Non-Maximum Suppression (NMS). Moreover, in training phase, all three sub-networks are trained with their associated task-specific loss functions (as given in Eq. (2) and Eq. (3)) in unified training settings, the weighted sum of each loss is used to train the overall PCL-Former model as given in Eq. 4. While testing, the Classification-Former and Localization-Former operate on the candidate segments identified by the Proposal-Former as shown in Figure 3.

Loss Functions: For candidate segments (having actions not background) generation and action classification tasks, we have used softmax loss to train the *Proposal-Former* and *Classification-Former*. Mathematically, the softmax loss can be expressed as follows:

$$\mathcal{L}_{softmax} = \frac{1}{N} \sum_n (-\log(P_n^{a_n})) \quad (2)$$

Here, P is the probability vector, containing prediction voting for each class (P_n prediction probability of n^{th} class). To train the *Localization-Former* for action localization task, we utilized a specialized loss function called *Overlap Loss* introduced in Shou et al. (2016). This function inherently incorporates Intersection over Union (IoU) with ground truth instances, enhancing the model’s capacity to discern segments with higher overlaps, thereby optimizing subsequent selection processes. Mathematically, the overlap loss can be equated as follows:

$$\mathcal{L}_{Overlap} = \frac{1}{N} \sum_n \left(\frac{1}{2} \cdot \left(\frac{(P_n^{a_n})^2}{(v_n)^\alpha} - 1 \right) \right) \quad (3)$$

Where a_n is the action category of n^{th} instance in a segment. In case of *Proposal-Former* $a_{n=1}$ refers to action and $a_{n=0}$ refers to background. While in the case of *Classification-Former* a_n indicates the n^{th} action category. Thus, the overlap loss serves the purpose of improving the temporal boundary prediction scores P for segments that exhibit maximum overlaps with the ground truth instances while diminishing the scores for those with minimal overlaps. The hyper-parameter α regulates the degree of confidence score. For unified training, the aforementioned losses are combined as follows:

$$\mathcal{L}_{total} = \mathcal{L}_{softmax} + \lambda \cdot \mathcal{L}_{Overlap} \quad (4)$$

Here, the hyper-parameter λ ensures the balance contribution of each loss in the final loss \mathcal{L}_{total} .

4 EXPERIMENTS AND RESULTS

To evaluate the effectiveness of the proposed PCL-Former, we have conducted extensive experiments on three commonly used benchmark datasets. First, we briefly describe the datasets used in this work, followed by the evaluation metrics used for quantitative evaluation. Next, we briefly discuss the implementation details and experimental settings.

4.1 DATASETS

We conducted experiments on three TAL benchmark datasets, which include THUMOS14 Idrees et al. (2017), ActivityNet-1.3 Caba Heilbron et al. (2015), and HACS Zhao et al. (2019) dataset. The **THUMOS14** dataset contains 413 untrimmed videos containing 20 temporally annotated actions. Following Gao et al. (2022), we used 200 untrimmed videos for training and the remaining 213 for testing/evaluation. The **ActivityNet-1.4** dataset contains 20,000 untrimmed videos spanning across 200 action categories. These videos are distributed among training, validation, and testing sets in

a ratio of 2:1:1, respectively. Following Lin et al. (2018); Zhang et al. (2022), We train our model using the training set and evaluate its performance on the validation set. The **HACS** dataset contains 140K complete action segments across 50,000 videos. Following the standard training protocol, we use the training set and evaluate the model on the validation set.

4.2 EVALUATION METRICS

We used Mean Average Precision (mAP) as the performance evaluation metric for quantitative assessment and comparison with state-of-the-art approaches. To better generalize the performance of our method, we evaluated the temporal action localization task with different tIoU thresholds. For the THUMOS14 dataset, we used a set of tIoU thresholds including {0.1, 0.2, 0.3, 0.4, 0.5, 0.6, 0.7}. For ActivityNet-1.3 and the HACS dataset, we used tIoU thresholds including {0.5, 0.75, 0.95}.

4.3 IMPLEMENTATION DETAILS

All experiments are conducted on a Linux-based (Ubuntu) machine having a 3.4GHz processor (40 cores), 128GB of onboard RAM, and two Tesla P4 8GB GPUs operated with CUDA 11.3. Further, the proposed method is implemented in PyTorch V1.12 using a well-known codebase MMAAction2 Contributors (2020). The proposed PCL-Former is trained for 100 epochs on the THUMOS14 dataset using TSN Wang et al. (2016) and I3D Carreira & Zisserman (2017) backbones with a learning rate 1e-4, batch size 1 (single untrimmed video), and a weight decay of 1e-4. Similarly, for ActivityNet-1.3 and the HACS dataset, we have trained our model for 100 epochs using I3D Carreira & Zisserman (2017) backbone with a learning rate 1e-4, batch size 1 and a weight decay of 1e-4. It is worth noting here that we have used only RGB videos from each dataset to train our PCL-Former. Further, we ablated our method in detail to assess the impact of different tIoU thresholds in NMS, the impact of individual modules, and the impact of segment length. It is worth mentioning here that the Temporal Intersection Over Union (tIoU) threshold for NMS is set to 0.4 for THUMOS14 and 0.5 for ActivityNet1.3 and the HACS dataset.

4.4 COMPARISON WITH STATE-OF-THE-ART

THUMOS14: The quantitative results tabulated in Table 1 presents a detailed comparative analysis of our method against several state-of-the-art approaches over the THUMOS14 dataset, evaluating mAP values across varying IoU thresholds from 0.1 to 0.7, i.e., {0.1:0.1:0.7}. Notably, our method outperforms the state-of-the-art TAL methods by obtaining the best mAP values with I3D Carreira & Zisserman (2017) backbone and the second-best mAP values with TSN Wang et al. (2016) backbone.

ActivityNet-1.3: The quantitative results listed in the rightmost column of Table 1 also compare our method (with I3D backbone) against the state-of-the-art TAL approaches on ActivityNet-1.3 dataset. The mAP values are compared using three different tIoU thresholds, including 0.5, 0.75, and 0.95. Our method outperforms the state-of-the-art TAL methods, specifically recent works that include TALLFormer Cheng & Bertasius (2022), ActionFormer Zhang et al. (2022), ASL Shao et al. (2023), TriDet Shi et al. (2023), Re²TAL Zhao et al. (2023), and ViT-TAD Yang et al. (2023) method, by obtaining the best average mAP of 38.2.

HACS: Table 2 presents the comparison of our method with the state-of-the-art TAL methods on HACS dataset. The mAP values are compared using three different tIoU thresholds that include 0.5, 0.75, and 0.95. The tabulated mAP values demonstrate the effectiveness of our method, outperforming the state-of-the-art TAL methods on the HACS dataset by obtaining the best mAP values across all tIoU thresholds. Overall, our proposed method outperforms the existing TAL methods on THUMOS14, ActivityNet-1.3, and the HACS dataset. These improvements demonstrate the efficacy and potential of our approach for localizing/detecting actions in long-untrimmed videos.

4.5 ABLATION STUDY

Table 1: **Comparison** of our **PCL-Former** with state-of-the-art TAL methods on **THUMOS14** and **ActivityNet-1.3** dataset. Results are compared using mAP (%) at different tIoU thresholds and average mAP (%). Best mAP values are listed in **bold** and runner-up in underlined.

| Model | Backbone | Venue | THUMOS14 | | | | | | | ActivityNet1.3 | | | | |
|--|--------------|-------|----------|------|------|------|------|------|------|----------------|------|------|------|------|
| | | | 0.1 | 0.2 | 0.3 | 0.4 | 0.5 | 0.6 | 0.7 | Avg. | 0.5 | 0.75 | 0.95 | Avg. |
| S-CNN Shou et al. (2016) | — | CVPR | 47.7 | 43.5 | 36.3 | 28.7 | 19.0 | — | — | 19.0 | — | — | — | — |
| SSN Zhao et al. (2017) | TSN | ICCV | 60.3 | 56.2 | 50.6 | 40.8 | 29.1 | — | — | 47.4 | 43.2 | 28.7 | 5.6 | 25.8 |
| TAG Xiong et al. (2017) | TSN | ARXIV | 64.1 | 57.7 | 48.7 | 39.8 | 28.2 | — | — | 47.7 | 41.1 | 24.1 | 5.0 | 23.4 |
| TALNet Chao et al. (2018) | I3D | CVPR | 59.8 | 57.1 | 53.2 | 48.5 | 42.8 | 33.8 | 20.8 | 45.1 | 38.2 | 18.3 | 1.3 | 19.2 |
| BSN Lin et al. (2018) | TSN | ECCV | — | — | 53.5 | 45.0 | 36.9 | 28.4 | 20.0 | 36.8 | 46.5 | 30.0 | 8.0 | 28.1 |
| GTAN Long et al. (2019) | P3D | CVPR | 69.1 | 63.7 | 57.8 | 47.2 | 38.8 | — | — | 55.3 | 52.6 | 34.1 | 8.9 | 31.8 |
| BMN Lin et al. (2019) | TSN | ICCV | 56.0 | 47.4 | 38.8 | 29.7 | 20.5 | — | — | 38.5 | 50.1 | 34.8 | 8.9 | 31.2 |
| PGCN Zeng et al. (2019) | I3D | ICCV | — | — | — | — | — | — | — | 48.3 | 33.2 | 31.1 | 3.3 | 22.5 |
| GTAD Xu et al. (2020) | TSN | CVPR | 66.4 | 60.4 | 51.6 | 37.6 | 22.9 | — | — | 47.8 | 50.4 | 34.6 | 9.0 | 31.3 |
| BC-GNN Bai et al. (2020) | I3D | ECCV | — | — | — | — | — | — | — | — | 50.6 | 34.8 | 9.4 | 31.6 |
| BU-TAL Zhao et al. (2020) | TSN | ECCV | 53.9 | 50.7 | 45.4 | 38.0 | 28.5 | — | — | 43.3 | 43.5 | 33.9 | 9.2 | 28.8 |
| A2Net Yang et al. (2020) | I3D | TIP | 61.1 | 60.2 | 58.6 | 54.1 | 45.5 | 32.5 | 17.2 | 47.0 | 43.6 | 28.7 | 3.7 | 25.3 |
| PCG-TAL Su et al. (2020) | I3D | TIP | 71.2 | 68.9 | 65.1 | 59.5 | 51.2 | — | — | 63.2 | 44.3 | 29.9 | 5.5 | 26.5 |
| BSN++ Su et al. (2021) | TSN | AAAI | — | — | 59.9 | 49.5 | 41.3 | 31.9 | 22.8 | 41.1 | 51.3 | 35.7 | 9.0 | 32.0 |
| TCA-Net Qing et al. (2021) | TSN | CVPR | — | — | 60.6 | 53.2 | 44.6 | 36.8 | 26.7 | 44.4 | 52.3 | 36.7 | 6.9 | 31.9 |
| RTD-Action Tan et al. (2021) | TSN | ICCV | — | — | 68.3 | 62.3 | 51.9 | 38.8 | 23.7 | 49.0 | 47.2 | 30.7 | 8.6 | 28.8 |
| ContextLoc Zhu et al. (2021) | I3D | ICCV | — | — | 68.3 | 63.8 | 54.3 | 41.8 | 26.2 | 50.9 | 56.0 | 35.2 | 3.6 | 34.2 |
| VSGN Zhao et al. (2021) | TSN | ICCV | — | — | 66.7 | 60.4 | 52.4 | 41.0 | 30.4 | 50.2 | 52.3 | 35.2 | 8.3 | 31.9 |
| AFSD Lin et al. (2021) | I3D | CVPR | — | — | 67.3 | 62.4 | 55.5 | 43.7 | 31.1 | 52.0 | 52.4 | 35.3 | 6.5 | 31.4 |
| Sub-Action Wang et al. (2021a) | I3D | TCSVT | 66.1 | 60.0 | 52.3 | 43.2 | 32.9 | — | — | 50.9 | 37.1 | 24.1 | 5.8 | 22.3 |
| RCL Wang et al. (2022) | TSN | CVPR | — | — | 70.1 | 62.3 | 52.9 | 42.7 | 30.7 | 51.7 | — | — | — | — |
| DCAN Chen et al. (2022) | TSN | AAAI | — | — | 68.2 | 62.7 | 54.1 | 43.9 | 32.6 | 52.3 | — | — | — | — |
| SRF-Net Ou et al. (2022) | I3D | JSC | — | 53.9 | 56.5 | 50.7 | 44.8 | 33.0 | 20.9 | 41.2 | — | — | — | — |
| TAL-MTS Gao et al. (2022) | I3D | ARXIV | 75.3 | 73.8 | 70.5 | 65.0 | 56.9 | 46.0 | 32.7 | 61.2 | 52.4 | 34.7 | 6.0 | 31.0 |
| TadTR Liu et al. (2022a) | I3D | TIP | — | — | 74.8 | 69.1 | 60.1 | 46.6 | 32.8 | 56.7 | 53.6 | 37.5 | 10.5 | 36.7 |
| TALLFormer Cheng & Bertasius (2022) | I3D | ECCV | — | — | 68.4 | — | 57.6 | — | 30.8 | 53.9 | 41.3 | 27.3 | 6.3 | 24.9 |
| ActionFormer Zhang et al. (2022) | I3D | ECCV | — | — | 82.1 | 77.8 | 71.0 | 59.4 | 43.9 | 66.8 | 53.5 | 36.2 | 8.2 | 35.6 |
| TriDet Shi et al. (2023) | I3D R(2+1)D | CVPR | — | — | 83.6 | 80.1 | 72.9 | 62.4 | 47.4 | 69.3 | 54.7 | 38.0 | 8.4 | 36.8 |
| ASL Shao et al. (2023) | I3D | ICCV | — | — | 83.1 | 79.0 | 71.7 | 59.7 | 45.8 | 67.9 | 54.1 | 37.4 | 8.0 | 36.2 |
| Re ² TAL Zhao et al. (2023) | I3D | CVPR | — | — | 77.4 | 72.6 | 64.9 | 53.7 | 39.0 | — | 55.2 | 37.8 | 9.0 | 37.0 |
| ViT-TAD Yang et al. (2023) | ViT-B | ARXIV | — | — | 85.1 | 80.9 | 74.2 | 61.8 | 45.4 | 69.5 | 55.8 | 38.4 | 8.8 | 37.4 |
| LFA Tang et al. (2024) | I3D | TIP | — | — | 83.0 | 79.5 | 73.8 | 62.5 | 48.2 | 69.4 | 54.7 | 37.3 | 8.6 | 36.6 |
| EEl Mokari & Sadeghi (2024) | TSN | IVC | 66.2 | 62.6 | 56.7 | 48.8 | 39.3 | — | — | — | 37.8 | 28.3 | 5.1 | 27.2 |
| DeTAL Li et al. (2024b) | I3D | TPAMI | — | — | 39.8 | 33.6 | 25.9 | 17.4 | 9.9 | 25.3 | 39.3 | 26.4 | 5.0 | 25.8 |
| EPN Wu et al. (2024) | I3D | TNNLS | 72.5 | 67.1 | 58.5 | 48.0 | 37.1 | 25.7 | 13.6 | — | 41.4 | 25.1 | 6.2 | 25.2 |
| NGPLG Li et al. (2024a) | I3D | TIP | 77.9 | 73.9 | 66.6 | 59.4 | 48.6 | 36.7 | 22.7 | 55.1 | 41.3 | 30.9 | 4.8 | 26.5 |
| ISSF Yun et al. (2024) | I3D | AAAI | 72.4 | 66.9 | 58.4 | 49.7 | 41.8 | 25.5 | 12.8 | 46.8 | 39.4 | 25.8 | 6.4 | 25.8 |
| CausalTAD Liu et al. (2024a) | I3D TSP | ARXIV | — | — | 84.4 | 80.7 | 73.5 | 62.7 | 47.4 | 69.7 | 55.6 | 38.5 | 9.4 | 37.4 |
| AdaTAD Liu et al. (2024b) | SlowFast-R50 | CVPR | — | — | 84.5 | 80.2 | 71.6 | 60.9 | 46.9 | 68.8 | 56.1 | 38.9 | 9.0 | 37.8 |
| PCL-Former (ours) | TSN | — | 87.9 | 86.4 | 85.7 | 81.4 | 75.3 | 63.9 | 49.1 | 75.6 | 55.7 | 38.4 | 9.7 | 37.6 |
| PCL-Former (ours) | I3D | — | 89.6 | 88.3 | 86.8 | 84.5 | 77.2 | 68.6 | 54.1 | 78.4 | 56.3 | 39.1 | 11.7 | 38.6 |

Impact of Different tIoU Thresholds in NMS: To evaluate the impact of tIoU threshold on overall performance of our method, we follow the settings in Xu et al. (2017) and Gao et al. (2022) and examine the performance of our method with four different tIoU thresholds that include $\{0.2, 0.3, 0.4, \text{ and } 0.5\}$ in NMS on THUMOS14,

ActivityNet-1.3, and HACS dataset. Table 3a, 3b, and 3c illustrate the impact of various tIoUs in NMS on the overall performance of PCL-Former on THUMOS14, ActivityNet-1.3, and HACS dataset, respectively.

Impact of Individual Modules: To study the effect of individual modules, we investigated the performance of PCL-Former on THUMOS14, ActivityNet-1.3, and HACS dataset under four different settings including CL-Former (excluding Proposal-Former), PC-Former (excluding Localization-Former), PCL-Former_(w/oBRM), and PCL-Former_(complete). The obtained quan-

Table 2: **Comparison** of our PCL-Former (I3D backbone) with state-of-the-art TAL methods on **HACS** dataset. The results are compared using mAP(%) at different tIoU thresholds and average mAP(%).

| Method | 0.5 | 0.75 | 0.95 | Avg |
|--------------------------------------|-------------|-------------|-------------|-------------|
| S-2D-TAN Zhang et al. (2019) | - | - | - | 23.4 |
| GTAD Xu et al. (2020) | - | - | - | 27.5 |
| BMN Lin et al. (2019) | 52.5 | 36.4 | 10.4 | 35.8 |
| TALL-Former Cheng & Bertasius (2022) | 55.0 | 36.1 | 11.8 | 36.5 |
| TadTR Liu et al. (2022a) | 47.1 | 32.1 | 10.9 | 30.0 |
| TCA-NET Qing et al. (2021) | <u>56.7</u> | <u>41.1</u> | <u>12.1</u> | <u>39.7</u> |
| TriDet-I3D Shi et al. (2023) | 54.5 | 36.8 | 11.5 | 36.8 |
| TriDet-SlowFast Shi et al. (2023) | 56.7 | 39.3 | 11.7 | 38.6 |
| PCL-Former (ours) | 61.2 | 47.9 | 16.4 | 44.5 |

Table 3: **Impact** of different tIoU thresholds in NMS on the performance of our **PCL-Former**, over (a) THUMOS14, (b) ActivityNet-1.3, and (c) HACS dataset.

(a) **Impact** of different tIoU thresholds in NMS on mAP values (%) over **THUMOS14** dataset.

| tIoU Thresholds | | mAP (%) | | | | | | | |
|-----------------|-----|-------------|-------------|-------------|-------------|-------------|-------------|-------------|-------------|
| | | 0.1 | 0.2 | 0.3 | 0.4 | 0.5 | 0.6 | 0.7 | Avg |
| 0.2 | TSN | 86.2 | 85.4 | 84.6 | 80.5 | 74.3 | 62.5 | 47.7 | 74.4 |
| 0.3 | | 87.4 | <u>86.1</u> | 85.5 | 80.7 | 74.4 | 63.4 | 48.5 | 75.1 |
| 0.4 | | 87.9 | 86.4 | 85.7 | 81.4 | 75.3 | 63.9 | 49.1 | 75.6 |
| 0.5 | | 87.8 | 85.9 | 85.4 | 80.8 | <u>74.5</u> | <u>63.5</u> | 48.9 | <u>75.2</u> |
| 0.2 | I3D | 88.3 | 87.7 | 86.1 | 83.4 | 76.4 | 67.5 | 52.6 | 77.4 |
| 0.3 | | 88.8 | 88.0 | 86.7 | 84.1 | 76.7 | 68.1 | <u>53.5</u> | 77.9 |
| 0.4 | | 89.6 | 88.3 | 86.8 | 84.5 | 77.2 | 68.6 | 54.1 | 78.4 |
| 0.5 | | 89.0 | <u>88.2</u> | 86.4 | <u>84.2</u> | 76.8 | <u>68.4</u> | 53.4 | 78.1 |

(b) **Impact** of different tIoU thresholds in NMS on mAP values (%) over **ActivityNet-1.3** dataset. (c) **Impact** of different tIoU thresholds in NMS on mAP values (%) over **HACS** dataset.

| tIoU Thresholds | mAP (%) | | | | tIoU Thresholds | mAP (%) | | | |
|-----------------|-------------|-------------|-------------|-------------|-----------------|-------------|-------------|-------------|-------------|
| | 0.5 | 0.75 | 0.95 | Avg | | 0.5 | 0.75 | 0.95 | Avg |
| 0.2 | <u>55.7</u> | 37.8 | 10.1 | 37.0 | 0.2 | 60.3 | 46.8 | 15.8 | 43.6 |
| 0.3 | 55.2 | 38.2 | 10.8 | 37.2 | 0.3 | <u>60.9</u> | 47.1 | <u>16.1</u> | 44.0 |
| 0.4 | 55.5 | 38.1 | 10.4 | 37.1 | 0.4 | 60.6 | <u>47.3</u> | 16.0 | 43.9 |
| 0.5 | 56.3 | 39.1 | 11.7 | 38.6 | 0.5 | 61.2 | 47.9 | 16.4 | 44.5 |

Table 4: **Impact** of individual modules of PCL-Former on the overall performance in terms of Avg mAP on **THUMOS14**, **ActivityNet-1.3**, and **HACS** dataset. Here, P-Former, C-Former, and L-Former represent Proposal-Former, Classification-Former, and Localization-Former, respectively.

| Method | Backbone | P-Former | C-Former | L-Former | BRM | Avg |
|----------------------------------|----------|----------|----------|----------|-----|-------------|
| THUMOS14 | | | | | | |
| CL-Former | TSN | | ✓ | ✓ | ✓ | 72.0 |
| PC-Former | | ✓ | ✓ | | ✓ | 70.2 |
| PCL-Former _(w/o BRM) | | ✓ | ✓ | ✓ | | <u>73.4</u> |
| PCL-Former _(complete) | | ✓ | ✓ | ✓ | ✓ | 75.6 |
| CL-Former | I3D | | ✓ | ✓ | ✓ | 75.3 |
| PC-Former | | ✓ | ✓ | | ✓ | 73.2 |
| PCL-Former _(w/o BRM) | | ✓ | ✓ | ✓ | | 76.8 |
| PCL-Former _(complete) | | ✓ | ✓ | ✓ | ✓ | 78.4 |
| ActivityNet-1.3 | | | | | | |
| CL-Former | I3D | | ✓ | ✓ | ✓ | 35.1 |
| PC-Former | | ✓ | ✓ | | ✓ | 33.0 |
| PCL-Former _(w/o BRM) | | ✓ | ✓ | ✓ | | <u>36.6</u> |
| PCL-Former _(complete) | | ✓ | ✓ | ✓ | ✓ | 38.6 |
| HACS | | | | | | |
| CL-Former | I3D | | ✓ | ✓ | ✓ | 41.4 |
| PC-Former | | ✓ | ✓ | | ✓ | 39.3 |
| PCL-Former _(w/o BRM) | | ✓ | ✓ | ✓ | | <u>42.9</u> |
| PCL-Former _(complete) | | ✓ | ✓ | ✓ | ✓ | 44.5 |

titative results in terms of average mAP values are presented in Table 4. The first setting (i.e., CL-Former) excludes Proposal-Former and operates directly on a sliding window. The second setting (i.e., PC-Former) excludes Localization-Former and operates on foreground sequence (prediction from Proposal-Former) to predict the action. The action class probabilities are utilized to predict the action boundaries. Third setting PCL-Former_(w/o BRM) does not utilize the BRM module in a post-processing step. The last setting utilizes the complete PCL-Former architecture for temporal action localization tasks. The listed mAP values in Table 4 demonstrate the effectiveness of the individual module in PCL-Former architecture.

Impact of Segment Length: To investigate the impact of segment length on the performance of our proposed PCL-Former, we conducted experiments with four different segment lengths including 16, 32, 64, and 128 over THUMOS14, ActivityNet-1.3, and HACS dataset. The obtained results with different segment lengths are presented in Table 5a, 5b, and 5c. Observing the results on the THUMOS14 dataset in Table 5a, it can be noticed that our PCL-Former (with both backbones TSN and I3D) obtains the best average mAP values using segment length of 64 and second-best average mAP values with segment length 32. Similarly, on ActivityNet-1.3 and HACS dataset in Table 5b and 5c, the proposed method achieves optimal results using a segment length of 64

Table 5: **Impact** of different temporal lengths of segments on the performance of our **PCL-Former**, over (a) THUMOS14, (b) ActivitNet-1.3, and (c) HACS dataset.

(a) **Impact** of different segment lengths on mAP values (%) over **THUMOS14** dataset.

| Segment Length | | mAP (%) | | | | | | | |
|----------------|-----|-------------|-------------|-------------|-------------|-------------|-------------|-------------|-------------|
| | | 0.1 | 0.2 | 0.3 | 0.4 | 0.5 | 0.6 | 0.7 | Avg |
| 16 | TSN | 86.2 | 83.8 | 83.3 | 78.8 | 72.2 | 63.0 | 47.1 | 73.4 |
| 32 | | 87.6 | 85.1 | 84.9 | 79.7 | 73.9 | 63.6 | 47.8 | 74.6 |
| 64(*) | | 87.9 | 86.4 | 85.7 | 81.4 | 75.3 | 63.9 | 49.1 | 75.6 |
| 128 | | 86.7 | 84.6 | 83.6 | 79.4 | 73.4 | 63.5 | 47.7 | 74.1 |
| 16 | IBD | 86.9 | 86.2 | 84.6 | 81.4 | 74.9 | 66.3 | 51.0 | 75.9 |
| 32 | | 88.3 | 87.1 | 85.2 | 83.3 | 76.1 | 67.4 | 51.8 | 77.0 |
| 64(*) | | 89.6 | 88.3 | 86.8 | 84.5 | 77.2 | 68.6 | 54.1 | 78.4 |
| 128 | | 87.3 | 86.0 | 85.0 | 81.8 | 76.0 | 67.0 | 51.4 | 76.3 |

(b) **Impact** of different segment lengths on mAP values (%) over **ActivityNet-1.3** dataset.

| Segment Length | mAP (%) | | | |
|----------------|-------------|-------------|-------------|-------------|
| | 0.5 | 0.75 | 0.95 | Avg |
| 16 | 53.4 | 35.6 | 10.2 | 35.5 |
| 32 | 55.5 | 38.3 | 11.3 | 37.5 |
| 64(*) | 56.3 | 39.1 | 11.7 | 38.6 |
| 128 | 53.8 | 37.2 | 10.9 | 36.4 |

| Segment Length | mAP (%) | | | |
|----------------|-------------|-------------|-------------|-------------|
| | 0.5 | 0.75 | 0.95 | Avg |
| 16 | 58.6 | 46.3 | 14.3 | 42.4 |
| 32 | 59.9 | 47.5 | 14.8 | 43.4 |
| 64(*) | 61.2 | 47.9 | 16.4 | 44.5 |
| 128 | 59.2 | 46.1 | 14.6 | 42.6 |

(annotated with * in Table 5a, 5b, and 5c) and obtains the second-best average mAP values with a segment length of 32.

5 CONCLUSION

Precise temporal action localization in untrimmed videos remains a critical yet challenging task in the context of human action detection. Untrimmed videos typically contain multiple action instances, often interspersed with irrelevant content such as background scenes or unrelated activities. To address these complexities, we thoroughly explore the inherent rich spatio-temporal properties of transformers in multi-stage settings for temporal action localization. This exploration leads to the development of a novel, three-tier transformer-based architecture, named PCL-Former, designed specifically for the temporal action localization task. PCL-Former consists of three task-specific transformer modules, each paired with a dedicated loss function to handle distinct sub-tasks. Specifically, the Proposal-Former identifies candidate segments that may contain actions, the Classification-Former classifies the action category in a given segment, and the Localization-Former predicts the temporal boundaries of the action instance (start and end of action). During training, each sub-network is independently trained with its respective loss, while inferring, the Classification-Former, and Localization-Former operate on the candidate segments identified by the Proposal-Former. Extensive experiments on THUMOS14, ActivityNet-1.3, and HACS demonstrate that PCL-Former outperforms state-of-the-art TAL methods on all datasets. Additionally, we conduct thorough ablation studies, analyzing the impact of different IoU thresholds in NMS, the impact of individual module, and the impact of segment length. The resulting mAP values provide deeper insights into the architecture’s configuration and the effectiveness of its components.

ACKNOWLEDGMENT

This research was supported in part by the Air Force Office of Scientific Research (AFOSR) Contract Number FA9550-22-1-0040. The authors would like to acknowledge Dr. Erik Blasch from the Air Force Research Laboratory (AFRL) for his guidance and support on the project. Any opinions, findings, and conclusions or recommendations expressed in this material are those of the author(s) and do not necessarily reflect the views of the Air Force, the Air Force Research Laboratory (AFRL), and/or AFOSR.

REFERENCES

- Anurag Arnab, Mostafa Dehghani, Georg Heigold, Chen Sun, Mario Lučić, and Cordelia Schmid. Vivit: A video vision transformer. In *Proceedings of the IEEE/CVF international conference on computer vision*, pp. 6836–6846, 2021.
- Yueran Bai, Yingying Wang, Yunhai Tong, Yang Yang, Qiyue Liu, and Junhui Liu. Boundary content graph neural network for temporal action proposal generation. In *Computer Vision–ECCV 2020: 16th European Conference, Glasgow, UK, August 23–28, 2020, Proceedings, Part XXVIII 16*, pp. 121–137. Springer, 2020.
- Gedas Bertasius, Heng Wang, and Lorenzo Torresani. Is space-time attention all you need for video understanding? In *ICML*, volume 2, pp. 4, 2021.
- Fabian Caba Heilbron, Victor Escorcia, Bernard Ghanem, and Juan Carlos Niebles. Activitynet: A large-scale video benchmark for human activity understanding. In *Proceedings of the IEEE conference on computer vision and pattern recognition*, pp. 961–970, 2015.
- Nicolas Carion, Francisco Massa, Gabriel Synnaeve, Nicolas Usunier, Alexander Kirillov, and Sergey Zagoruyko. End-to-end object detection with transformers. In *European conference on computer vision*, pp. 213–229. Springer, 2020.
- Joao Carreira and Andrew Zisserman. Quo vadis, action recognition? a new model and the kinetics dataset. In *proceedings of the IEEE Conference on Computer Vision and Pattern Recognition*, pp. 6299–6308, 2017.
- Shuning Chang, Pichao Wang, Fan Wang, Hao Li, and Zheng Shou. Augmented transformer with adaptive graph for temporal action proposal generation. In *Proceedings of the 3rd International Workshop on Human-Centric Multimedia Analysis*, pp. 41–50, 2022.
- Yu-Wei Chao, Sudheendra Vijayanarasimhan, Bryan Seybold, David A Ross, Jia Deng, and Rahul Sukthankar. Rethinking the faster r-cnn architecture for temporal action localization. In *Proceedings of the IEEE conference on computer vision and pattern recognition*, pp. 1130–1139, 2018.
- Guo Chen, Yin-Dong Zheng, Limin Wang, and Tong Lu. Dcan: improving temporal action detection via dual context aggregation. In *Proceedings of the AAAI conference on artificial intelligence*, volume 36, pp. 248–257, 2022.
- Feng Cheng and Gedas Bertasius. Tallformer: Temporal action localization with a long-memory transformer. In *European Conference on Computer Vision*, pp. 503–521. Springer, 2022.
- MMAAction2 Contributors. Openmmlab’s next generation video understanding toolbox and benchmark. <https://github.com/open-mmlab/mmaaction2>, 2020.
- Rui Dai, Srijan Das, Kumara Kahatapitiya, Michael S Ryoo, and François Brémond. Ms-tct: multi-scale temporal convtransformer for action detection. In *Proceedings of the IEEE/CVF Conference on Computer Vision and Pattern Recognition*, pp. 20041–20051, 2022.
- Alexey Dosovitskiy, Lucas Beyer, Alexander Kolesnikov, Dirk Weissenborn, Xiaohua Zhai, Thomas Unterthiner, Mostafa Dehghani, Matthias Minderer, Georg Heigold, Sylvain Gelly, et al. An image is worth 16x16 words: Transformers for image recognition at scale. *arXiv preprint arXiv:2010.11929*, 2020.
- Haoqi Fan, Bo Xiong, Karttikeya Mangalam, Yanghao Li, Zhicheng Yan, Jitendra Malik, and Christoph Feichtenhofer. Multiscale vision transformers. In *Proceedings of the IEEE/CVF international conference on computer vision*, pp. 6824–6835, 2021.
- Gueter Josmy Faure, Min-Hung Chen, and Shang-Hong Lai. Holistic interaction transformer network for action detection. In *Proceedings of the IEEE/CVF winter conference on applications of computer vision*, pp. 3340–3350, 2023.
- Jiyang Gao, Zhenheng Yang, Kan Chen, Chen Sun, and Ram Nevatia. Turn tap: Temporal unit regression network for temporal action proposals. In *Proceedings of the IEEE international conference on computer vision*, pp. 3628–3636, 2017.

-
- Zan Gao, Xinglei Cui, Tao Zhuo, Zhiyong Cheng, An-An Liu, Meng Wang, and Shenyong Chen. Temporal action localization with multi-temporal scales. *arXiv preprint arXiv:2208.07493*, 2022.
- Haroon Idrees, Amir R Zamir, Yu-Gang Jiang, Alex Gorban, Ivan Laptev, Rahul Sukthankar, and Mubarak Shah. The thumos challenge on action recognition for videos “in the wild”. *Computer Vision and Image Understanding*, 155:1–23, 2017.
- Tae-Kyung Kang, Gun-Hee Lee, Kyung-Min Jin, and Seong-Whan Lee. Action-aware masking network with group-based attention for temporal action localization. In *Proceedings of the IEEE/CVF Winter Conference on Applications of Computer Vision*, pp. 6058–6067, 2023.
- Guozhang Li, De Cheng, Nannan Wang, Jie Li, and Xinbo Gao. Neighbor-guided pseudo-label generation and refinement for single-frame supervised temporal action localization. *IEEE Transactions on Image Processing*, 2024a.
- Zhiheng Li, Yujie Zhong, Ran Song, Tianjiao Li, Lin Ma, and Wei Zhang. Detal: open-vocabulary temporal action localization with decoupled networks. *IEEE Transactions on Pattern Analysis and Machine Intelligence*, 2024b.
- Chuming Lin, Chengming Xu, Donghao Luo, Yabiao Wang, Ying Tai, Chengjie Wang, Jilin Li, Feiyue Huang, and Yanwei Fu. Learning salient boundary feature for anchor-free temporal action localization. In *Proceedings of the IEEE/CVF Conference on Computer Vision and Pattern Recognition*, pp. 3320–3329, 2021.
- Tianwei Lin, Xu Zhao, and Zheng Shou. Single shot temporal action detection. In *Proceedings of the 25th ACM international conference on Multimedia*, pp. 988–996, 2017.
- Tianwei Lin, Xu Zhao, Haisheng Su, Chongjing Wang, and Ming Yang. Bsn: Boundary sensitive network for temporal action proposal generation. In *Proceedings of the European conference on computer vision (ECCV)*, pp. 3–19, 2018.
- Tianwei Lin, Xiao Liu, Xin Li, Errui Ding, and Shilei Wen. Bmn: Boundary-matching network for temporal action proposal generation. In *Proceedings of the IEEE/CVF international conference on computer vision*, pp. 3889–3898, 2019.
- Shuming Liu, Lin Sui, Chen-Lin Zhang, Fangzhou Mu, Chen Zhao, and Bernard Ghanem. Harnessing temporal causality for advanced temporal action detection. *arXiv preprint arXiv:2407.17792*, 2024a.
- Shuming Liu, Chen-Lin Zhang, Chen Zhao, and Bernard Ghanem. End-to-end temporal action detection with 1b parameters across 1000 frames. In *Proceedings of the IEEE/CVF conference on computer vision and pattern recognition*, pp. 18591–18601, 2024b.
- Xiaolong Liu, Qimeng Wang, Yao Hu, Xu Tang, Shiwei Zhang, Song Bai, and Xiang Bai. End-to-end temporal action detection with transformer. *IEEE Transactions on Image Processing*, 31: 5427–5441, 2022a.
- Ze Liu, Jia Ning, Yue Cao, Yixuan Wei, Zheng Zhang, Stephen Lin, and Han Hu. Video swin transformer. In *Proceedings of the IEEE/CVF conference on computer vision and pattern recognition*, pp. 3202–3211, 2022b.
- Fuchen Long, Ting Yao, Zhaofan Qiu, Xinmei Tian, Jiebo Luo, and Tao Mei. Gaussian temporal awareness networks for action localization. In *Proceedings of the IEEE/CVF conference on computer vision and pattern recognition*, pp. 344–353, 2019.
- Mozhgan Mokari and Khosrow Haj Sadeghi. Enhancing temporal action localization in an end-to-end network through estimation error incorporation. *Image and Vision Computing*, 145:104994, 2024.
- Zhilong Ou, YanMin Luo, Jin Chen, and Geng Chen. Srfnet: selective receptive field network for human pose estimation. *The Journal of Supercomputing*, 78(1):691–711, 2022.

-
- Zhiwu Qing, Haisheng Su, Weihao Gan, Dongliang Wang, Wei Wu, Xiang Wang, Yu Qiao, Junjie Yan, Changxin Gao, and Nong Sang. Temporal context aggregation network for temporal action proposal refinement. In *Proceedings of the IEEE/CVF conference on computer vision and pattern recognition*, pp. 485–494, 2021.
- Jiayi Shao, Xiaohan Wang, Ruijie Quan, Junjun Zheng, Jiang Yang, and Yi Yang. Action sensitivity learning for temporal action localization. In *Proceedings of the IEEE/CVF International Conference on Computer Vision*, pp. 13457–13469, 2023.
- Dingfeng Shi, Yujie Zhong, Qiong Cao, Lin Ma, Jia Li, and Dacheng Tao. Tridet: Temporal action detection with relative boundary modeling. In *Proceedings of the IEEE/CVF Conference on Computer Vision and Pattern Recognition*, pp. 18857–18866, 2023.
- Zheng Shou, Dongang Wang, and Shih-Fu Chang. Temporal action localization in untrimmed videos via multi-stage cnns. In *Proceedings of the IEEE conference on computer vision and pattern recognition*, pp. 1049–1058, 2016.
- Zheng Shou, Jonathan Chan, Alireza Zareian, Kazuyuki Miyazawa, and Shih-Fu Chang. Cdc: Convolutional-de-convolutional networks for precise temporal action localization in untrimmed videos. In *Proceedings of the IEEE conference on computer vision and pattern recognition*, pp. 5734–5743, 2017.
- Haisheng Su, Weihao Gan, Wei Wu, Yu Qiao, and Junjie Yan. Bsn++: Complementary boundary regressor with scale-balanced relation modeling for temporal action proposal generation. In *Proceedings of the AAAI conference on artificial intelligence*, volume 35, pp. 2602–2610, 2021.
- Rui Su, Dong Xu, Lu Sheng, and Wanli Ouyang. Pcg-tal: Progressive cross-granularity cooperation for temporal action localization. *IEEE Transactions on Image Processing*, 30:2103–2113, 2020.
- Jing Tan, Jiaqi Tang, Limin Wang, and Gangshan Wu. Relaxed transformer decoders for direct action proposal generation. In *Proceedings of the IEEE/CVF international conference on computer vision*, pp. 13526–13535, 2021.
- Yepeng Tang, Weining Wang, Chunjie Zhang, Jing Liu, and Yao Zhao. Learnable feature augmentation framework for temporal action localization. *IEEE Transactions on Image Processing*, 2024.
- Du Tran, Lubomir Bourdev, Rob Fergus, Lorenzo Torresani, and Manohar Paluri. Learning spatiotemporal features with 3d convolutional networks. In *Proceedings of the IEEE international conference on computer vision*, pp. 4489–4497, 2015.
- Du Tran, Heng Wang, Lorenzo Torresani, Jamie Ray, Yann LeCun, and Manohar Paluri. A closer look at spatiotemporal convolutions for action recognition. In *Proceedings of the IEEE conference on Computer Vision and Pattern Recognition*, pp. 6450–6459, 2018.
- Ashish Vaswani, Noam Shazeer, Niki Parmar, Jakob Uszkoreit, Llion Jones, Aidan N Gomez, Łukasz Kaiser, and Illia Polosukhin. Attention is all you need. *Advances in neural information processing systems*, 30, 2017.
- Binglu Wang, Xun Zhang, and Yongqiang Zhao. Exploring sub-action granularity for weakly supervised temporal action localization. *IEEE Transactions on Circuits and Systems for Video Technology*, 32(4):2186–2198, 2021a.
- Limin Wang, Yuanjun Xiong, Zhe Wang, Yu Qiao, Dahua Lin, Xiaoou Tang, and Luc Van Gool. Temporal segment networks: Towards good practices for deep action recognition. In *European conference on computer vision*, pp. 20–36. Springer, 2016.
- Lining Wang, Haosen Yang, Wenhao Wu, Hongxun Yao, and Hujie Huang. Temporal action proposal generation with transformers. *arXiv preprint arXiv:2105.12043*, 2021b.
- Qiang Wang, Yanhao Zhang, Yun Zheng, and Pan Pan. Rcl: Recurrent continuous localization for temporal action detection. In *Proceedings of the IEEE/CVF Conference on Computer Vision and Pattern Recognition*, pp. 13566–13575, 2022.

-
- Kewei Wu, Wenjie Luo, Zhao Xie, Dan Guo, Zhao Zhang, and Richang Hong. Ensemble prototype network for weakly supervised temporal action localization. *IEEE Transactions on Neural Networks and Learning Systems*, 2024.
- Yuanjun Xiong, Yue Zhao, Limin Wang, Dahua Lin, and Xiaoou Tang. A pursuit of temporal accuracy in general activity detection. *arXiv preprint arXiv:1703.02716*, 2017.
- Huijuan Xu, Abir Das, and Kate Saenko. R-c3d: Region convolutional 3d network for temporal activity detection. In *Proceedings of the IEEE international conference on computer vision*, pp. 5783–5792, 2017.
- Mengmeng Xu, Chen Zhao, David S Rojas, Ali Thabet, and Bernard Ghanem. G-tad: Sub-graph localization for temporal action detection. In *Proceedings of the IEEE/CVF conference on computer vision and pattern recognition*, pp. 10156–10165, 2020.
- Le Yang, Houwen Peng, Dingwen Zhang, Jianlong Fu, and Junwei Han. Revisiting anchor mechanisms for temporal action localization. *IEEE Transactions on Image Processing*, 29:8535–8548, 2020.
- Min Yang, Huan Gao, Ping Guo, and Limin Wang. Adapting short-term transformers for action detection in untrimmed videos. *arXiv preprint arXiv:2312.01897*, 2023.
- Wulian Yun, Mengshi Qi, Chuanming Wang, and Huadong Ma. Weakly-supervised temporal action localization by inferring salient snippet-feature. In *Proceedings of the AAAI conference on artificial intelligence*, volume 38, pp. 6908–6916, 2024.
- Runhao Zeng, Wenbing Huang, Mingkui Tan, Yu Rong, Peilin Zhao, Junzhou Huang, and Chuang Gan. Graph convolutional networks for temporal action localization. In *Proceedings of the IEEE/CVF international conference on computer vision*, pp. 7094–7103, 2019.
- Chen-Lin Zhang, Jianxin Wu, and Yin Li. Actionformer: Localizing moments of actions with transformers. In *European Conference on Computer Vision*, pp. 492–510. Springer, 2022.
- Gongjie Zhang, Zhipeng Luo, Zichen Tian, Jingyi Zhang, Xiaoqin Zhang, and Shijian Lu. Towards efficient use of multi-scale features in transformer-based object detectors. In *Proceedings of the IEEE/CVF conference on computer vision and pattern recognition*, pp. 6206–6216, 2023.
- Songyang Zhang, Houwen Peng, Le Yang, Jianlong Fu, and Jiebo Luo. Learning sparse 2d temporal adjacent networks for temporal action localization. *arXiv preprint arXiv:1912.03612*, 2019.
- Chen Zhao, Ali K Thabet, and Bernard Ghanem. Video self-stitching graph network for temporal action localization. In *Proceedings of the IEEE/CVF International Conference on Computer Vision*, pp. 13658–13667, 2021.
- Chen Zhao, Shuming Liu, Karttikeya Mangalam, and Bernard Ghanem. Re2tal: Rewiring pretrained video backbones for reversible temporal action localization. In *Proceedings of the IEEE/CVF Conference on Computer Vision and Pattern Recognition*, pp. 10637–10647, 2023.
- Hang Zhao, Antonio Torralba, Lorenzo Torresani, and Zhicheng Yan. Hacs: Human action clips and segments dataset for recognition and temporal localization. In *Proceedings of the IEEE International Conference on Computer Vision*, pp. 8668–8678, 2019.
- Jiaojiao Zhao, Yanyi Zhang, Xinyu Li, Hao Chen, Bing Shuai, Mingze Xu, Chunhui Liu, Kaustav Kundu, Yuanjun Xiong, Davide Modolo, et al. Tuber: Tubelet transformer for video action detection. In *Proceedings of the IEEE/CVF Conference on Computer Vision and Pattern Recognition*, pp. 13598–13607, 2022.
- Peisen Zhao, Lingxi Xie, Chen Ju, Ya Zhang, Yanfeng Wang, and Qi Tian. Bottom-up temporal action localization with mutual regularization. In *Computer Vision—ECCV 2020: 16th European Conference, Glasgow, UK, August 23–28, 2020, Proceedings, Part VIII 16*, pp. 539–555. Springer, 2020.

Yue Zhao, Yuanjun Xiong, Limin Wang, Zhirong Wu, Xiaoou Tang, and Dahua Lin. Temporal action detection with structured segment networks. In *Proceedings of the IEEE international conference on computer vision*, pp. 2914–2923, 2017.

Zixin Zhu, Wei Tang, Le Wang, Nanning Zheng, and Gang Hua. Enriching local and global contexts for temporal action localization. In *Proceedings of the IEEE/CVF international conference on computer vision*, pp. 13516–13525, 2021.

A APPENDIX TO EXPERIMENTS

A.1 CLASSWISE ACCURACY COMPARISON WITH STATE-OF-THE-ART

In addition to the quantitative comparison given in Section 4.4 (Comparison with State-of-the-Art), we further evaluated our PCL-Former by comparing its class-wise performance with the S-CNN Shou et al. (2016), CDC Shou et al. (2017), and AMNet Kang et al. (2023) on THUMOS14 dataset, as illustrated in Figure 4. As shown in Figure 4, our PCL-Former outperforms all other TAL methods by a significant margin, achieving the highest Average Precision (AP) across all classes. In terms of Mean Average Precision (mAP), our method achieves the highest performance, with a mAP of 78.4% followed by AMNet Kang et al. (2023), which attains the second-best mAP of 63.3%, demonstrating a substantial gap between our approach and the competing methods. It is worth mentioning here that all the references cited in this supplementary file are directly sourced from the main paper. This ensures consistency and allows readers to easily trace the original studies, methodologies, and related work discussed throughout the supplementary material.

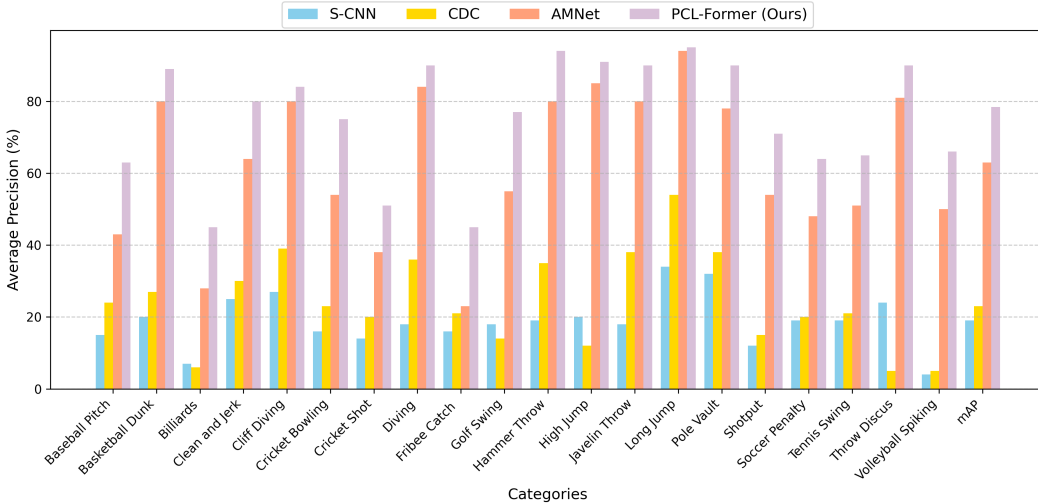


Figure 4: Class-wise performance comparison with S-CNN Shou et al. (2016), CDC Shou et al. (2017), and AMNet Kang et al. (2023) methods on THUMOS14 dataset. The results are evaluated using AP@Avg across various tIoU thresholds.

A.2 QUALITATIVE RESULTS

Besides quantitative evaluation, we further assessed our method’s performance in terms of temporal boundary prediction on the test set of the THUMOS14 dataset. This qualitative analysis aimed to evaluate the capability of our approach to accurately localize action instances by predicting their start and end times within video sequences. By examining the temporal alignment of predicted segments with ground truth annotations, we highlighted the precision and robustness of our method in handling complex temporal boundaries. For the qualitative evaluation, we selected four videos from the test set of the THUMOS14 dataset, corresponding to the actions **Javelin Throw**, **Hammer Throw**, **Long Jump**, and **Diving**. An overlap threshold of 0.4 is used during Non-Maximum Suppression (NMS) to identify the optimal temporal predictions for each action instance. The

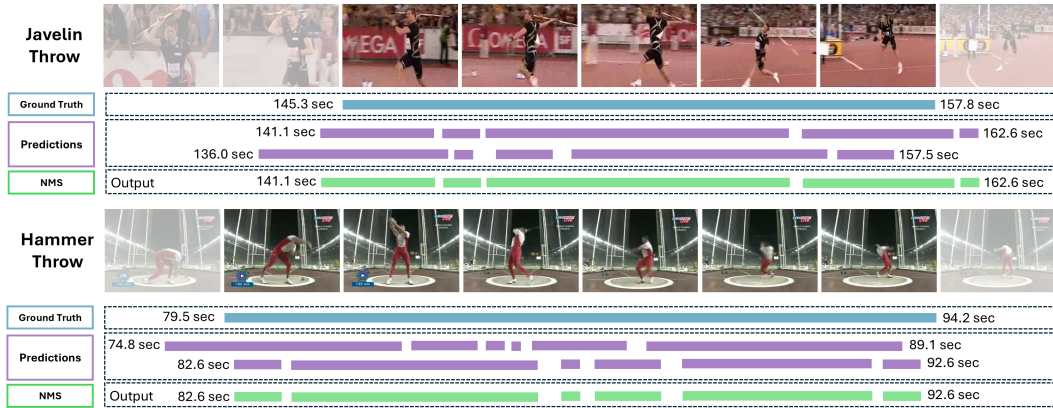


Figure 5: The prediction results for the **Javelin Throw** and **Hammer Throw** action instances from the THUMOS14 test set, evaluated using an overlap threshold of 0.4. For each ground truth instance, two predictions are provided. The NMS process is applied to both, selecting the prediction with the highest overlap with the ground truth.

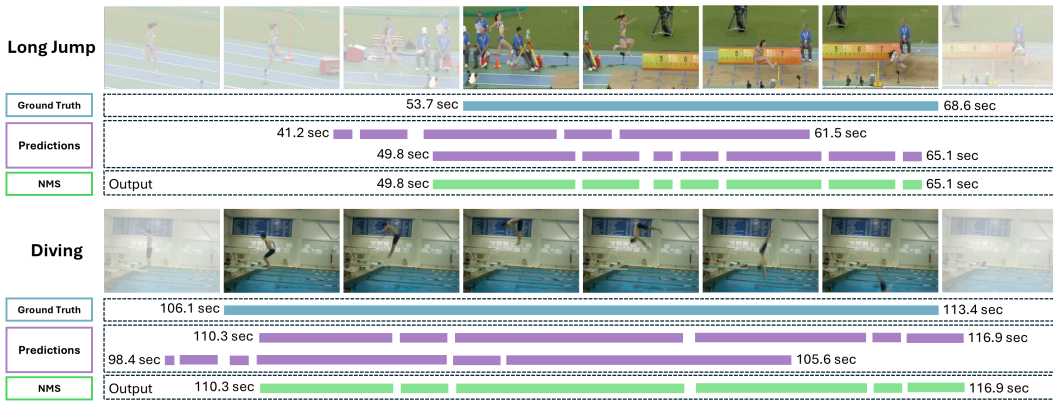


Figure 6: The prediction results for the **Long Jump** and **Diving** action instances from the THUMOS14 test set, evaluated using an overlap threshold of 0.4. For each ground truth instance, two predictions are provided. The NMS process is applied to both, selecting the prediction with the highest overlap with the ground truth.

resulting temporal predictions are illustrated in Figure 5 and Figure 6, highlighting the effectiveness of our method in capturing precise action boundaries.

Figure 5 depicts the temporal action localization results for Javelin Throw and Hammer Throw, from the THUMOS14 test set. The visualization includes three components: ground truth annotations, predicted temporal segments, and the final outputs after applying Non-Maximum Suppression (NMS). It is worth mentioning here that, we provided two distinct predictions for each ground truth instance. For example, in the case of the Javelin Throw, the first prediction spans from 141.1 seconds to 162.6 seconds, while the second prediction spans from 136.0 seconds to 157.5 seconds. By applying Non-Maximum Suppression (NMS), the prediction with the highest overlap with the ground truth (spanning from 145.3 seconds to 157.8 seconds) is selected as the optimal prediction, which in this case corresponds to the first prediction. Similarly, for the Hammer Throw, NMS identifies the second prediction as the optimal choice, demonstrating the effectiveness of the selection process in refining temporal action localization results.

Further, Figure 6 illustrates the qualitative results of our method on Long Jump and Diving. Each activity is accompanied by ground truth annotations, two predicted temporal intervals, and the final output selected by Non-Maximum Suppression (NMS). For the Long Jump, the ground truth spans from 53.7 seconds to 68.6 seconds. Among the two predicted intervals, spanning 41.2 seconds to 61.5 seconds and 49.8 seconds to 65.1 seconds, NMS identifies the second prediction as

optimal due to its higher overlap with the ground truth. Similarly, in the Diving activity, the ground truth spans from 106.1 seconds to 113.4 seconds. Of the two predicted intervals, spanning 98.4 seconds to 105.6 seconds and 110.3 seconds to 116.9 seconds, NMS selects the second interval as the optimal prediction. These results further emphasize the ability of our approach to refine temporal predictions and accurately align them with the ground truth boundaries.